Article

Cell Reports

The ULK3 Kinase Is Critical for Convergent Control of Cancer-Associated Fibroblast Activation by CSL and GLI

Graphical Abstract

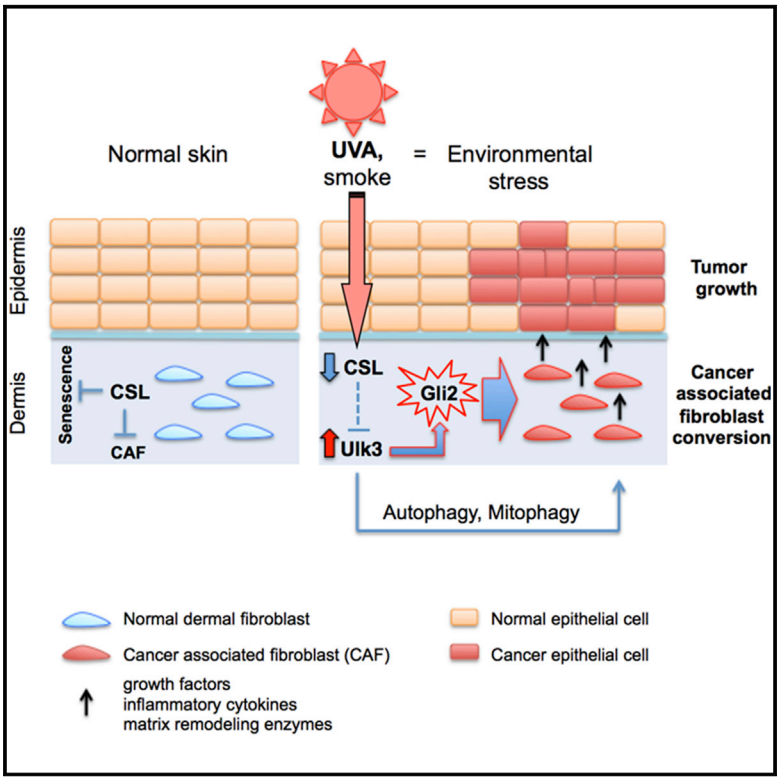

Highlights

- CAF conversion by loss of CSL depends on GLI activation
- CSL functions as a negative regulator of the pro-autophagy kinase ULK3
- Increased ULK3 induces GLI2-dependent CAF activation separately from autophagy
- Silencing of ULK3 in SCC-derived CAFs suppresses their tumor-enhancing properties

Authors

Sandro Goruppi, Maria-Giuseppina Procopio, Seunghee Jo, Andrea Clocchiatti, Victor Neel, G. Paolo Dotto

Correspondence

paolo.dotto@unil.ch

In Brief

Goruppi et al. demonstrate that CSL, a transcriptional repressor mediating Notch signaling, suppresses the conversion of fibroblasts into cancer-associated fibroblasts (CAFs) by controlling the expression of autophagy kinase ULK3, which, in turn, activates GLI signaling. Their studies connect two key pathways involved in CAF activation and identify a target for stroma-focused anti-cancer intervention.

Goruppi et al., 2017, Cell Reports *20*, 2468–2479
September 5, 2017
http://dx.doi.org/10.1016/j.celrep.2017.08.048

CellPress

OPEN ACCESS
CellPress

Cell Reports
Article

The ULK3 Kinase Is Critical for Convergent Control of Cancer-Associated Fibroblast Activation by CSL and GLI

Sandro Goruppi,[1,2] Maria-Giuseppina Procopio,[3] Seunghee Jo,[1,2] Andrea Clocchiatti,[1,2] Victor Neel,[4] and G. Paolo Dotto[1,3,5,*]

[1]Cutaneous Biology Research Center, Massachusetts General Hospital, 149 Bldg., 13th St. Charlestown, MA 02129, USA
[2]Department of Dermatology, Harvard Medical School, Boston, MA 02125, USA
[3]Department of Biochemistry, University of Lausanne, 155 Chemin des Boveresses, Epalinges 1066, Switzerland
[4]Department of Dermatology, Massachusetts General Hospital, Boston, MA 02114, USA
[5]Lead Contact
*Correspondence: paolo.dotto@unil.ch
http://dx.doi.org/10.1016/j.celrep.2017.08.048

SUMMARY

The connection between signaling pathways activating cancer-associated fibroblasts (CAFs) remains to be determined. Metabolic alterations linked to autophagy have also been implicated in CAF activation. CSL/RBPJ, a transcriptional repressor that mediates Notch signaling, suppresses the gene expression program(s), leading to stromal senescence and CAF activation. Deregulated GLI signaling can also contribute to CAF conversion. Here, we report that compromised CSL function depends on GLI activation for conversion of human dermal fibroblasts into CAFs, separately from cellular senescence. Decreased CSL upregulates the expression of the ULK3 kinase, which binds and activates GLI2. Increased ULK3 also induces autophagy, which is unlinked from GLI and CAF activation. ULK3 upregulation occurs in the CAFs of several tumor types, and ULK3 silencing suppresses the tumor-enhancing properties of these cells. Thus, ULK3 links two key signaling pathways involved in CAF conversion and is an attractive target for stroma-focused anti-cancer intervention.

INTRODUCTION

Stepwise acquisition of genetic alterations is implicated in epithelial tumor development, yet many of these changes can be found in apparently normal tissues, pointing to the importance of concomitant stromal changes (Bissell and Hines, 2011; Hanahan and Weinberg, 2011; Martincorena et al., 2015). Notch signaling controls cell-fate commitment, differentiation, and tumorigenesis (Allenspach et al., 2002; Artavanis-Tsakonas et al., 1999; Dotto, 2009). While Notch tumor-suppressive function in stratified epithelia is well established (Dotto, 2008), recent evidence indicates an opposite role in stromal fibroblasts (Hu et al., 2012; Junttila and de Sauvage, 2013; Procopio et al., 2015). Specifically, the CSL/RBP-Jκ protein (CSL), a transcriptional repressor mediating Notch signaling, is key for the negative control of cancer-associated fibroblast (CAF) activation. Deletion of the CSL gene in the mesenchymal skin compartment of mice results in multifocal keratinocyte tumor development preceded by dermal atrophy, matrix alterations, and inflammation (Hu et al., 2012). CSL loss in primary human fibroblasts results in a similar CAF phenotype that is associated with a p53-dependent program of cellular senescence (Procopio et al., 2015). The concomitant downmodulation of CSL and p53 activities leads to the expansion of altered stromal fibroblasts and cancer cells as seen in *field cancerization*, a condition of major clinical significance consistent of multiple and recurrent tumors (Dotto, 2014).

The Hedgehog (Hh) pathway is linked to the development of several types of epithelial cancers (Rubin and de Sauvage, 2006). A paracrine mechanism has been implicated in CAF activation, with Hh ligands secreted by cancer cells activating the glioma-associated transcription factors (Gli) in surrounding stromal cells (Junttila and de Sauvage, 2013; Theunissen and de Sauvage, 2009). Interestingly, while this chain of events should enhance tumor formation (Theunissen and de Sauvage, 2009), an opposite restraining function of stromal Hh activation in pancreatic and bladder cancer has also been reported (Özdemir et al., 2014; Rhim et al., 2014; Shin et al., 2014). Mammalian cells express three GLI proteins (Aberger and Ruiz i Altaba, 2014). Under basal conditions, glioma-associated transcription factor 2 (GLI2) is cleaved into a transcriptional repressor, with Hh stimulation blocking this process and converting it into an activator. Expression of glioma-associated transcription factor 1 (GLI1) is then induced as a signal amplifier. In *Drosophila*, the activation of GLI homolog Cubitus interruptus (Ci) is well established (Ruel et al., 2003; Wang et al., 2000), with a kinase (Fused) releasing it from an inhibitory complex (Costal2/SuFu) and promoting its nuclear translocation. In mammalian cells, the mechanisms responsible for GLI activation are less understood. Recently, the unc-51-like-kinase 3 (ULK3), an inducer in human fibroblasts of autophagy (Young et al., 2009), has been proposed to fulfill the role of Fused through association and phosphorylation of GLI2 (Maloverjan et al., 2010; Rubin and de Sauvage, 2006). Importantly, in cancer cells, GLI proteins can also be activated by Hh-receptor-independent mechanisms involving phosphatidylinositol 3-kinase (PI3K)/AKT (Metcalfe and de Sauvage, 2011), mitogen-activated protein

kinase (MAPK)/ERK (Seto et al., 2009), S6K (Wang et al., 2012), and KRAS activation (Nolan-Stevaux et al., 2009; Stecca et al., 2007).

Recent evidence suggests that altered metabolic properties of CAFs, resulting from increased autophagy/mitophagy and associated shift to aerobic glycolysis, can contribute to their tumor-enhancing properties (Kalluri, 2016; Martinez-Outschoorn et al., 2017). How these processes relate to CAFs activation remains to be determined. We report here an as-yet-unexpected link between the CSL and GLI signaling pathways, with the ULK3 kinase as an attractive target for stroma-focused anti-cancer intervention, controlling the CAF effector gene expression program separately from the autophagy/mitophagy processes.

RESULTS

CAF Conversion by Loss of CSL Function Depends on GLI Activation

The conversion of normal stromal fibroblasts into CAFs is likely to be a multistep process, with loss of CSL transcriptional repression inducing a large battery of CAF effector genes associated with stromal cell senescence, as a fail-safe mechanism limiting cancer/stromal cell expansion (Procopio et al., 2015). An unanswered question is the possible integration of different signaling(s) leading to CAF conversion. Like Notch/CSL, Hh-GLI signaling is deregulated in tumor stroma and can contribute to CAF activation (Junttila and de Sauvage, 2013; Theunissen and de Sauvage, 2009). Under basal conditions, GLI2 is cleaved into a transcriptional repressor, while block of this process coincides with GLI2 activation and induction of *GLI2* and *GLI1* expression as signal amplifiers (Aberger and Ruiz i Altaba, 2014). We found that, in human dermal fibroblasts (HDFs), the short repressive form of GLI2 was dramatically reduced, while the full-length transcription-activating protein was induced by shRNA-mediated *CSL* silencing (Figure 1A), at a time coinciding with the induction of CAF effector genes but preceding that of cellular senescence, (Procopio et al., 2015). In parallel, *GLI1* and *GLI2* expression was upregulated in HDFs and, to a similar extent, also in human gingival fibroblasts (HGFs) (Figures 1B, 1C, and S1A).

The aforementioned findings are of clinical and functional significance. Patient-derived CAFs have higher GLI2 levels than HDFs, which are inversely related to CSL expression (Figure 1D). Global analysis of gene expression of HDFs versus CAFs present notable similarities when compared to the expression profile after downmodulation of CSL function in HDFs (Procopio et al., 2015); thus, in our studies, we focused on a limited number of CAF genes to characterize the mechanism of HDF conversion to CAF. Functionally, induction of CAF effector genes by *CSL* knockdown was blocked in HDFs with concomitant *GLI2* silencing (Figure 1E) or in mouse embryo fibroblasts (MEFs) with disruption of the *gli1* and *gli2* genes (*gli* $1/2^{-/-}$) (Lipinski et al., 2008; Figures 1F and 1G). Notably, upregulation of senescent effectors by *CSL* loss was unaffected by *GLI2* silencing, thus implicating GLI activation selectively in the induction of CAF effector genes (Figures S1B and S1C).

An essential property of fibroblasts with deleted or silenced CSL is that they enhance the growth of adjacent cancer cells (Procopio et al., 2015). To test whether these properties are GLI dependent, we used a cancer/stromal cell expansion model that we developed, based on mouse ear injections of weakly tumorigenic squamous cell carcinoma (SCC) cells admixed with fibroblasts with various genetic manipulations (Procopio et al., 2015). We determined, every 3 days for 3 weeks, the growth of EGFP-expressing SCC13 cells admixed with *gli*$^{+/+}$ or *gli* $1/2^{-/-}$ MEFs, both with or without *Csl* silencing. As previously reported for HDFs with *CSL* silencing (Procopio et al., 2015), SCC13 cells admixed with *gli*$^{+/+}$ MEFs with *Csl* knockdown formed significantly larger lesions than controls (Figures 1H–1J), while the tumor-enhancing effects of *Csl* silencing were lost with MEFs with *gli1/2* gene deletion (Figures 1H–1J and S1E). Hence, our data indicate that CAF conversion of stromal fibroblasts by *CSL* loss requires GLI activity.

ULK3 Is a Direct CSL Target Gene that Links *CSL* Silencing to GLI and CAF Activation

In cancer cells, GLI proteins can be activated by Hh-receptor-dependent and -independent mechanisms (Aberger and Ruiz i Altaba, 2014). The ULK3 kinase was recently proposed to fulfill the same role in mammalian cells as the *Drosophila* Fused in GLI2 activation, through possible association and phosphorylation (Maloverjan et al., 2010; Rubin and de Sauvage, 2006). In agreement with these studies, we confirmed that ULK3 and GLI2 can be recovered by co-immunoprecipitation in ULK3-overexpressing cells, in which activated phosphorylated GLI2 (Xing et al., 2014) was detected (Figures 2A and 2B). We also determined the association of endogenous ULK3 and GLI2 by proximity ligation assays (PLAs) in HDFs in which ULK3 expression was increased by serum starvation (Figures 2C and 2D).

Upon *CSL* silencing, levels of *ULK3* expression were significantly induced in several HDFs strains, as well as in HGFs, while expression of two other family members, *ULK1* and *ULK2*, was unaffected (Figures 2E–2G and S2A–S2C). Notably, *ULK3* was also induced after *Csl* silencing in MEFs with *gli1/2* gene deletion (Figures 2H and 2I), in which the induction of CAF effector genes was blocked (Figures 1F and 1G). Bioinformatic analysis of the 5,000-bp promoter region of the ULK3 gene upstream of the initiating ATG revealed the presence of three putative CSL binding sites. Chromatin immunoprecipitation (ChIP) assays of HDFs showed little or no binding of CSL to the first upstream site (Site 1), while the other two were strongly bound, one upstream of the transcription start site (Site2) and the other in the first intron (Site3) (Figure 2J). Histone marks of active chromatin configuration (H3K27ac and H3K4me3) were highly enriched at these sites upon *CSL* knockdown (Figures 2K and S2D).

Upregulation of *ULK3* by *CSL* silencing is of functional significance, as GLI activation and induction of CAF effector genes were suppressed in cells with concomitant *CSL* and *ULK3* knockdown (Figure 3A). Consistent with previous reports (Maloverjan et al., 2010), we found that the activation of GLI reporter activation required ULK3 kinase activity in HDFs (Figure S2E). In contrast, determinants of cellular senescence (CDKN1A, CDKN2A, and CDKN2B) were induced by CSL loss also in concomitance with *ULK3* silencing (Figures S2F and S2G).

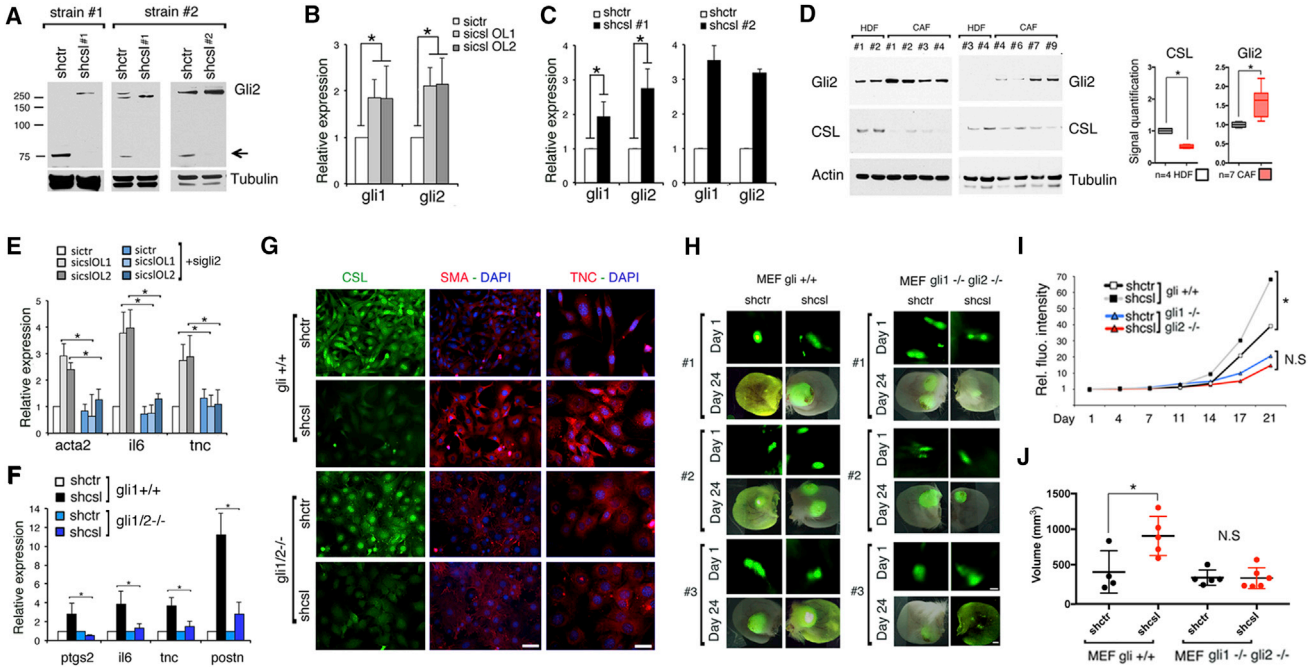

Figure 1. CAF Activation by CSL Silencing Depends on GLI Activation

(A) Immunoblot analysis of two HDFs strains with or without shRNA-mediated *CSL* silencing for 7 days with anti-GLI2 and γ-tubulin antibodies. The arrow points to the truncated GLI2 repressor form.

(B and C) qRT-PCR analysis of *GLI1* and *GLI2* expression in HDFs, with or without (B) siRNA-mediated or (C) shRNA-mediated *CSL* silencing. Data indicate mean ± SEM, three HDF strains, n (experiments) = 5 for sicsl OL1/2; n (experiments) = 3 for shcsl #1; n (experiments) = 2 in two HDF strains for shcsl #2. *p < 0.05, two-tailed unpaired t test. mean ± SD. Analysis of HGFs with or without *CSL* silencing is given in Figure S1A.

(D) Left: immunoblots with antibodies against indicated proteins of HDFs and CAFs. Right: immunoblot quantifications; data indicate mean ± SEM; n (HDFs) = 4; n (CAFs) = 7. *p < 0.05, two-tailed unpaired t test.

(E) qRT-PCR analysis of the indicated genes in HDFs with or without *CSL* and *GLI2* silencing as indicated. Data indicate mean ± SEM with two HDFs strains; n (experiments) = 3; *p < 0.05, two-tailed unpaired t test. Immunoblot analysis verifying *CSL* and *GLI2* silencing is given in Figure S1C.

(F) qRT-PCR analysis of the indicated genes in mouse embryo fibroblasts (MEFs) with *gli1* and *gli2* gene disruption (*gli 1/2*$^{-/-}$) (Lipinski et al., 2008) versus wild-type control (*gli*$^{+/+}$), stably infected with a *Csl* silencing versus control lentivirus for 2 weeks. Data indicate mean ± SEM; n (experiments) = 3; *p < 0.05, two-tailed unpaired t test.

(G) Immunofluorescence analysis of *gli*$^{+/+}$ versus *gli 1/2*$^{-/-}$ MEFs with or without shRNA-mediated *CSL* silencing as in (F), with the indicated antibodies and DAPI for nuclear staining. Scale bars, 60 μM for CSL and SMA and 30 μM for TNC.

(H–J) EGFP-expressing SCC13 cells were admixed with either *gli*$^{+/+}$ or *gli 1/2*$^{-/-}$ MEFs, stably infected with a *Csl* silencing or control lentivirus, followed by parallel injections into contralateral ears of SCID mice. (H) Images of combined bright-field and fluorescence microscopy of three mice per combination of cells, at days 1 and 21 after injection. (I) Increase of average fluorescence signals over time for all tumors per group. Quantification was achieved using ImageJ on images acquired every 3 days for 21 days, as in Procopio et al. (2015), and normalized to day1 after injection. n (tumors *gli*$^{+/+}$) = 4 for *shctr* and 5 for *shcsl*; n (tumors *gli 1/2*$^{-/-}$) = 5 for *shctr* and 6 for *shcsl*. For *gli 1/2*$^{+/+}$ MEF *shctr* versus *shcsl*, *p < 0.05; for *gli1/2*$^{-/-}$ MEF *shctr* versus *shcsl*, N.S (not significant), two-tailed equal variance unpaired t test. (J) Tumor volumes, measured as V = [(length × width^2) × 0.5], after 24 days from injection of admixed cells are indicated in (I). Median and SD are indicated. For *gli*$^{+/+}$ MEFs *shctr* versus *shcsl*, *p = 0.0091; and for *gli1/2*$^{-/-}$ MEFs *shctr* versus *shcsl*, N.S (not significant), unpaired samples, two-tailed equal variance t test. Scale bars, 30 μm for day 1 and 5 mm for day 21. The quantification comparing the lesions (*shcsl*/*shctr*) formed in the same animal is in Figure S1D.

See also Figure S1.

Conversely, increased *ULK3* expression by lentiviral infection was sufficient to induce *GLI* and CAF marker genes (Figures 3B and 3C), with induction of the latter being suppressed in cells with *GLI2* silencing (Figure 3D).

An important property of CAFs is the ability to enhance proliferation of neighboring cancer cells. In co-culture assays, proliferation of skin-derived SCC (SCC13) cells was enhanced to a much greater extent by HDFs with silencing of *CSL* individually than in combination with *ULK3* (Figures 3E and 3F). Thus, *ULK3* is a direct CSL target gene, which is required for GLI and CAF activation by *CSL* downmodulation.

CSL Silencing and Increased ULK3 Induce Cellular Autophagy and Mitophagy Separately from GLI and CAF Activation

Similarly to other ULK kinase family members, ULK3 can play a key role in the initiation of autophagy (Russell et al., 2013; Young et al., 2009). Consistent with the observed upregulation of *ULK3*, *CSL* silencing in HDFs induced autophagy, as assessed by a number of biochemical events, including processing of microtubule-associated protein-1 light chain 3 (LC3) (Klionsky et al., 2016), Beclin-1 phosphorylation (Russell et al., 2013), and down-modulation of the p62 cargo and TOM20 mitochondrial proteins

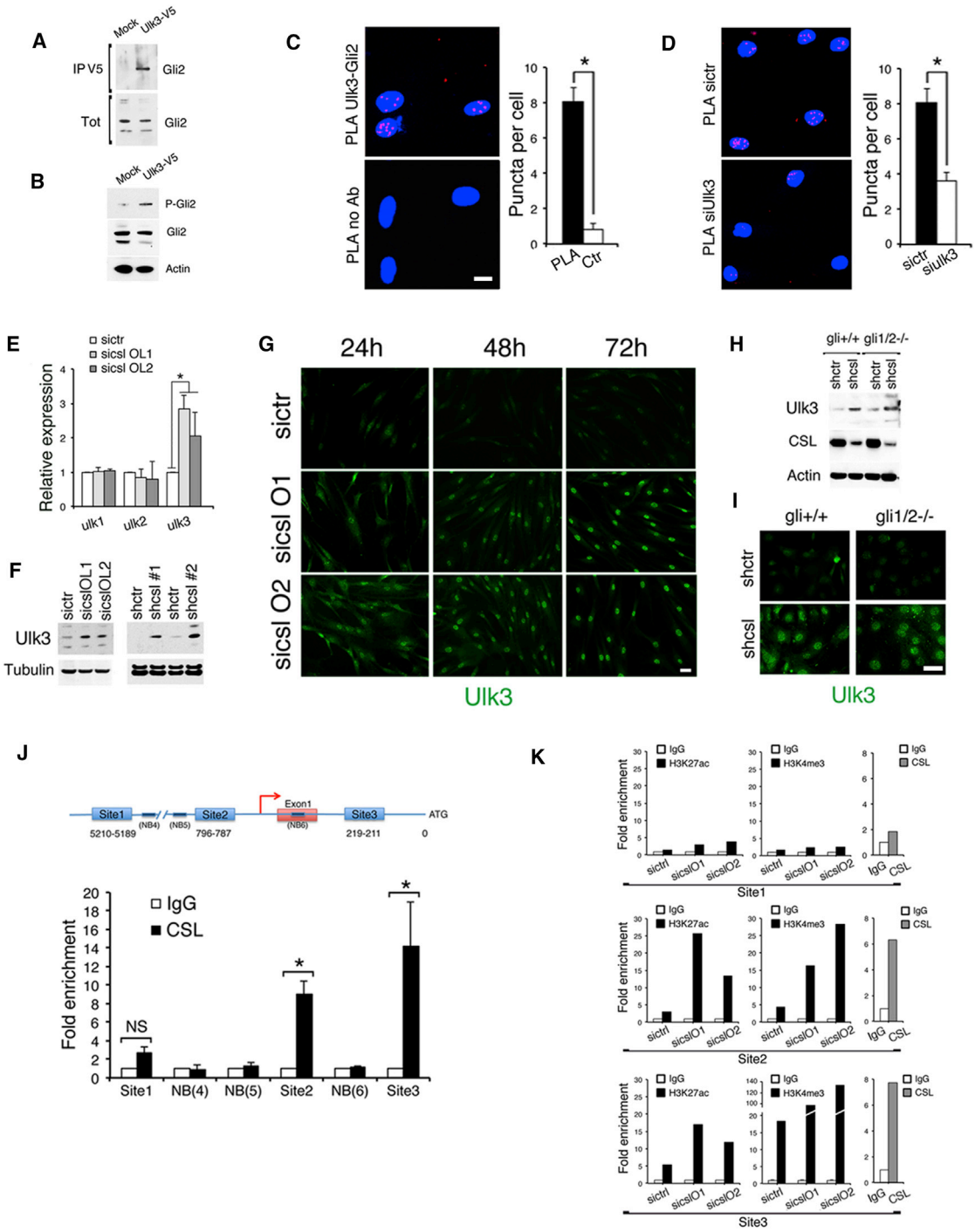

Figure 2. ULK3 Is a Direct CSL Target Gene that Links *CSL* Silencing to GLI Activation

(A) Immunoblot with anti-GLI2 antibodies of HEK293 cells transfected with an ULK3-V5 tag-expressing versus empty-vector control (Mock) after immunoprecipitation with anti-V5 antibodies with total input (Tot) as loading control.

(B) Immunoblot of total HEK293 extracts after transfection as in (A), with antibodies against activated phospho-GLI2 (Ser149) (Xing et al., 2014), GLI2, and β-actin.

(C and D) Proximity ligation assays (PLAs) with antibodies against ULK3 and GLI2 of HDFs serum starved for 24 hr for upregulation of endogenous ULK3. Assays without primary antibodies (no Ab) (C) or with cells with siRNA-mediated *ULK3* silencing (D) were used for specificity controls. Red fluorescence puncta resulting from juxtaposition of anti-ULK3 and -GLI2 antibodies were visualized by confocal microscopy with DAPI nuclear staining. Number of puncta per cell, n (cells) > 120 per condition; $p < 0.05$, two-tailed unpaired t test.

(legend continued on next page)

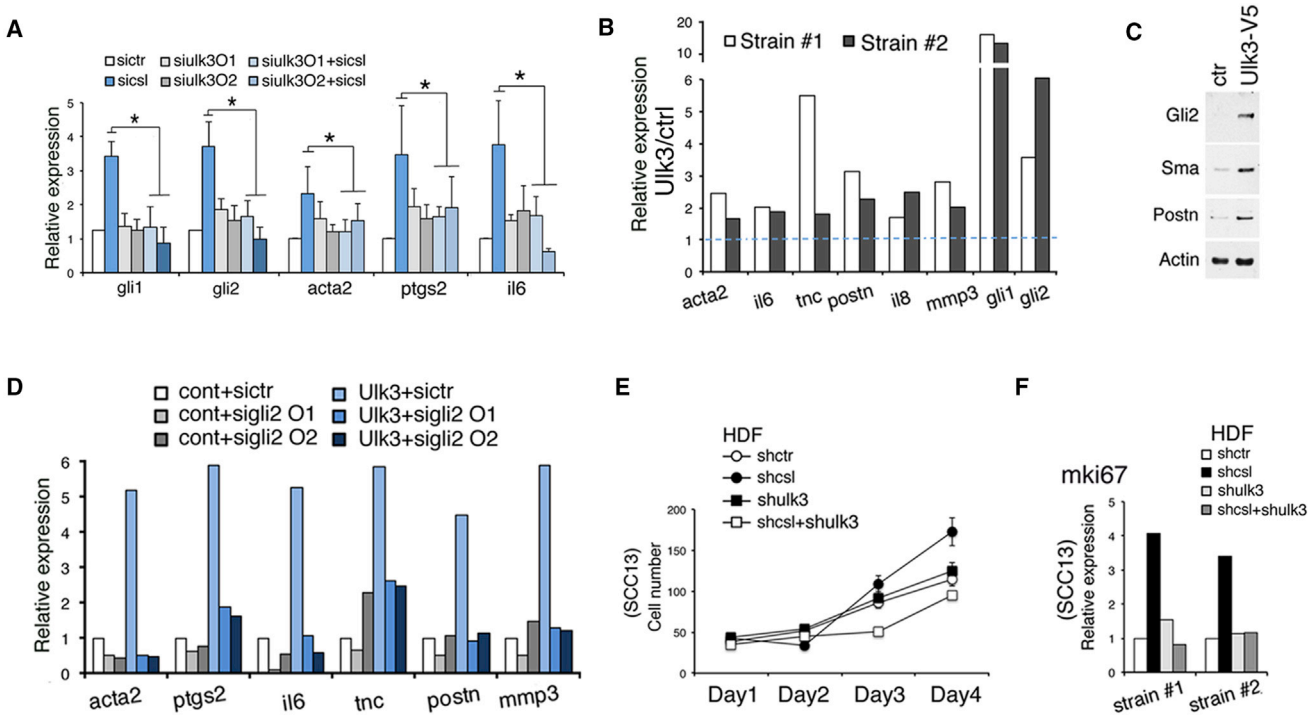

Figure 3. ULK3 Activity Is Required for Induction of GLI1/2 and CAF Effectors by *CSL* Silencing

(A) qRT-PCR analysis of the indicated genes in HDFs with or without *CSL* and *ULK3* silencing individually and in combination. Data indicate mean ± SEM with two HDF strains; n (experiments) = 3; *p < 0.05, two-tailed unpaired t test. An immunoblot analysis verifying *CSL* and *ULK3* silencing is shown in Figure S2G.

(B) qRT-PCR of the indicated genes in HDFs infected with *ULK3*-expressing versus empty-vector control lentiviruses. Results are expressed as folds of expression over control, after β-actin normalization. n (strains) = 2.

(C) Immunoblot of HDFs infected with same viruses as in (B), with antibodies against the indicated proteins.

(D) qRT-PCR of the indicated genes in HDFs infected with an ULK3-expressing (ULK3) versus control (cont) virus for 1 week, then with or without *GLI2* silencing for 48 hr (total, 9 days). Results are expressed as folds of expression in ULK3 overexpressing versus control.

(E) Cell counts of EGFP-SCC13 cells cultured for 4 days on well inserts with HDFs with or without *CSL* and/or *ULK3* silencing in the bottom. Duplicate cultures were photographed daily, and number of EGFP-SCC13 cells were quantified using ImageJ software. Data indicate mean ± SD.

(F) qRT-PCR analysis of *mki67* expression, normalized to β-actin, in SCC13 cells co-cultured for 4 days with two different HDFs strains with or without *CSL* and *ULK3* silencing as in (E). n (strains) = 2.

See also Figure S2.

(Bingol et al., 2014; Klionsky et al., 2016) (Figure 4A). Induction of these events was associated with an increase of autophagosome formation, which occurred also in HDFs with *CSL* silencing treated with the lysosomal inhibitor Bafilomycin, indicative of an enhanced "on rate" (Figures S3A–S3D). Cellular mitophagy is a selective form of autophagy with a decreased number of

(E) qRT-PCR analysis of *ulk1-3* expression in HDFs with or without siRNA-mediated *CSL* silencing with β-actin normalization. Data indicate mean ± SEM: n (experiments) = 5, three HDFs strains; *p < 0.05, two-tailed unpaired t test. qRT-PCR analyses of HDFs and human gingival fibroblasts (HGFs) with or without shRNA-mediated *CSL* silencing are given in Figures S2A and S2B.

(F) Immunoblot analysis of HDFs with or without siRNA- and shRNA-mediated *CSL* silencing with antibodies against ULK3 and γ-tubulin. Immunoblot analysis of HGFs with or without *CSL* silencing is given in Figure S2C.

(G) Immunofluorescence analysis of HDFs at various times (hours) from siRNA-mediated *CSL* silencing with antibodies against ULK3. Scale bar, 30 μm.

(H) Immunoblot analysis of $gli^{+/+}$ versus $gli1/2^{-/-}$ MEFs with or without shRNA-mediated *Csl* silencing with antibodies against ULK3 and β-actin.

(I) Immunofluorescence with anti-ULK3 antibodies of MEFs as in (H), Scale bar, 30 μm.

(J) Top: scheme of the human *ULK3* gene around the transcription start site (red arrow) and first non-coding exon with nucleotide position of predicted CSL binding sites (Site1, -2, -3) relative to the initiation codon (ATG) and non-binding regions (NB4, -5, -6). Bottom: Chromatin immunoprecipitation assays of HDFs with anti-CSL (CSL) or non-immune antibodies (immunoglobulin G; IgG) followed by binding determination of the indicated regions of the *ULK3* gene by qPCR. Results are expressed as enrichment fold relative to input; mean ± SEM, using two HDFs strains; n (experiments) = 3; *p < 0.05, two-tailed unpaired t test; NS, not significant.

(K) Chromatin immunoprecipitation assays (ChIPs) at the CSL binding sites in of HDFs with or without *CSL* silencing, with antibodies against active histone marks (H3K27Ac27 and H3K4me3) versus non-immune immunoglobulin G (IgG) (black and white bars, respectively) for the CSL binding sites at the *ULK3* promoter region. Parallel chromatin immunoprecipitation assays with anti-CSL antibodies of HDFs are shown (gray and white bars). Results obtained using a different HDF strain are given in Figure S2D.

See also Figure S2.

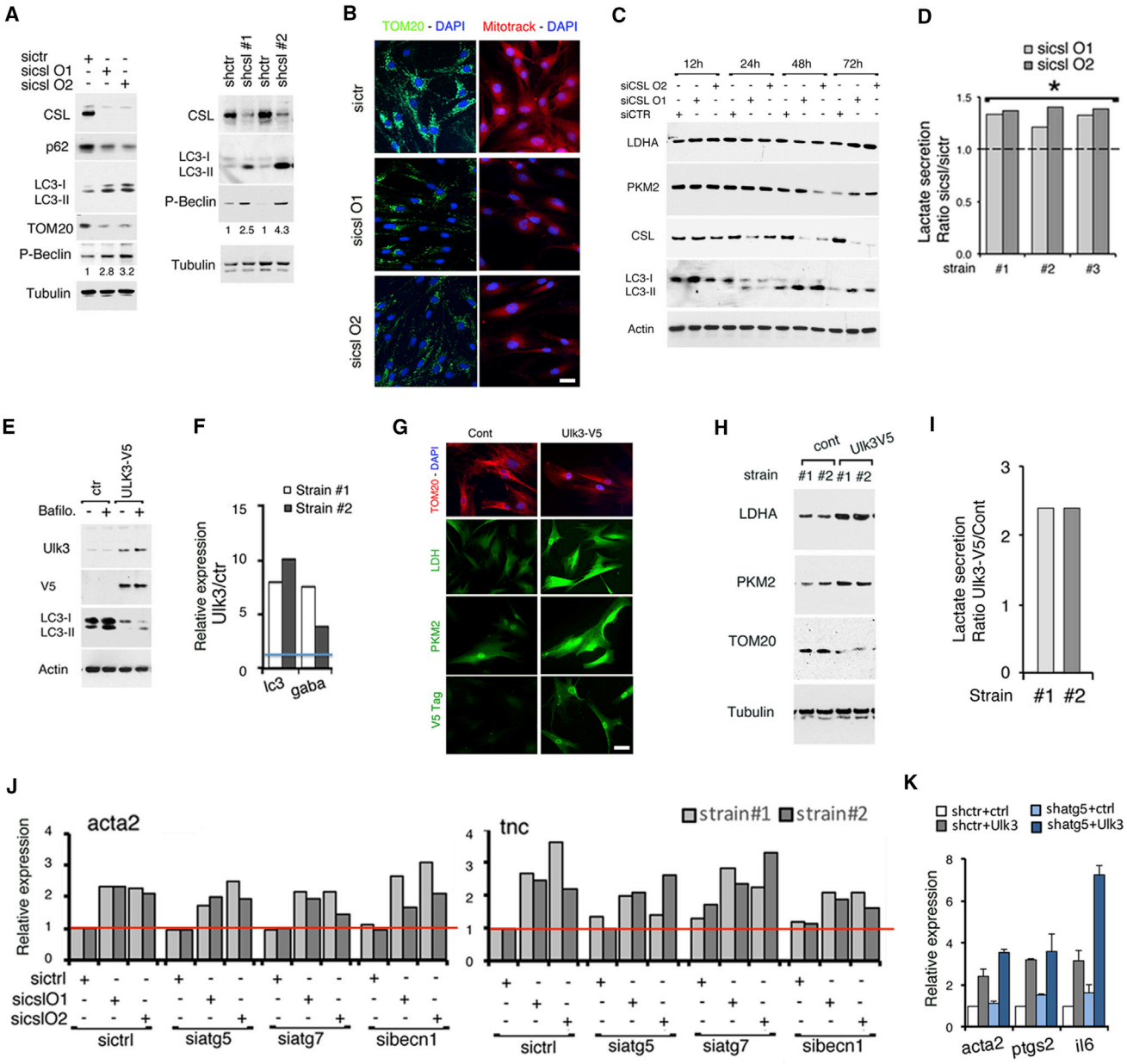

Figure 4. *CSL* Silencing and Increased ULK3 Induce Cellular Autophagy and Mitophagy Separately from GLI and CAF Activation

(A) Immunoblot analysis with antibodies against indicated proteins of HDFs with or without *CSL* silencing with siRNAs for 48 hr (left panel) or shRNAs for 1 week (right panel). Numbers refer to densitometric quantification (folds of induction) of phospho-Beclin1 in *CSL*-silenced versus control cells. Immunofluorescent analysis of endogenous puncta formation with or without *sicsl* and of red-fluorescent-protein-expressing HDFs with or without *sicsl* and with or without Bafilomycin are in Figures S3A–S3C. Western blot of LC3 processing with or without *sicsl* and with or without Bafilomycin is given in Figure S3D.

(B) Immunofluorescence analysis with anti-TOM20 antibodies or MitoTracker Deep Red FM staining (right and left panels, respectively) of HDFs with or without *CSL* silencing with siRNAs for 3 days. Scale bar, 10 μm.

(C) Immunoblot analysis of HDFs with or without *CSL* silencing with siRNAs for 3 days using antibodies against indicated proteins.

(D) Lactate secretion in culture medium of three HDFs strains with or without siRNA *CSL* silencing for 3 days. Results are expressed as the ratio *sicsl*/*sictr*, normalized for cell numbers. n (strains) = 3; *p < 0.05, one-sample t test.

(E) Immunoblot with antibodies against indicated proteins of HDFs infected with ULK3-V5-expressing versus control viruses (7 days) with or without Bafilomycin (400 nM) (last 4 hr of the experiment).

(F) qRT-PCR of the indicated genes in two HDF strains infected with ULK3-V5-expressing versus control viruses. Results are expressed as relative folds of expression over control, n (strains) = 2.

(G) Immunofluorescence analysis of HDFs infected with ULK3-V5-expressing versus control viruses, using antibodies against TOM20, LDH, PKM2 and V5-tag. Scale bar, 30 μm.

(legend continued on next page)

mitochondria leading to a metabolic shift toward aerobic glycolysis (Martinez-Outschoorn et al., 2017). After *CSL* silencing, both the mitochondrial TOM20 immunofluorescence signal and mitochondrial labeling with MitoTracker were decreased (Figure 4B). Consistent with enhanced mitophagy and glycolytic transition, HDFs with silenced *CSL* had enhanced expression of pyruvate kinase isozyme 2 (PKM2) and lactate dehydrogenase A (LDHA), two key enzymes responsible for lactate production (Figure 4C) and higher lactate levels (Figure 4D). A similar induction of autophagy, decreased mitochondria network, and increased glycolytic switch were observed in HDFs with increased *ULK3* expression (Figures 4E–4I).

An important question is whether the aforementioned processes are linked to induction of the CAF effector gene program or proceed as parallel independent events. Indicative of the second possibility, we found that the silencing of *CSL* induced CAF effector genes to a similar extent in HDFs with or without silencing of the autophagy-essential genes *ATG5*, *ATG7*, or *BECN1* (Figure 4J) and in MEFs with *Atg5* gene knockout, compared to wild-type MEFs (Figure S3E). Similarly, increased *ULK3* expression by lentiviral infection induced CAF effector genes in HDFs with silenced *ATG5* (Figure 4K). Thus, both *CSL* silencing and *ULK3* upregulation enhance autophagy, which is, however, dispensable for CAF effector gene induction.

ULK3 as a Target to Suppress CAF Activation and Cancer/Stromal Cell Expansion

An important question was whether *ULK3* expression is increased also in clinically occurring CAFs. Analysis of published gene expression profiles of CAFs derived from head and neck SCCs (HNSCCs) showed that expression of *ULK3* and *GLI* is consistently higher than in normal fibroblasts derived from the same body site, with similar upregulation in CAFs from prostate (Ashida et al., 2012) and breast (Finak et al., 2008) cancers (Figures 5A and S4A).

In skin, laser capture micro-dissection (LCM) followed by qRT-PCR analysis showed consistently increased *ULK3* expression in several SCC-adjacent stromal cells (in areas we tested as devoid of macrophage and leukocyte contamination; Procopio et al., 2015), relative to stroma areas of distant normal skin (Figure 5B). Results were confirmed by immunofluorescence analysis, showing a significantly higher number of ULK3-expressing fibroblasts (Vimentin-positive cells) in SCCs surrounding stroma versus unaffected areas of same or different individuals (Figures 5C and S4B). Similarly upregulated *ULK3* and *GLI* levels—with concomitantly decreased *CSL*—were also found in CAFs isolated from skin SCCs relative to normal dermal fibroblasts from same or different individuals (Figures 5D–5F and S4C). Results were further validated in a mouse model of actinic keratosis (AK) based on mesenchymal deletion of the *Csl* gene (Hu et al., 2012). LCM and qRT-PCR analysis showed significant *Ulk3* upregulation in stromal fibroblasts of skin lesions that developed in these mice at 3 months of age, relative to distant unaffected skin (Figure 5G).

To assess whether the observed increase in *ULK3* expression and GLI activation in CAFs is functionally linked to decreased *CSL*, we infected these cells with a *CSL*-inducible lentivirus that we previously showed to suppress CAF marker expression (Procopio et al., 2015). As shown in Figure 5H, increased *CSL* expression caused a significant downregulation of *ULK3* and *GLI* levels.

A much-needed development for cancer therapy is the identification of strategies affecting cancer stroma (Goruppi and Dotto, 2013). We found that siRNA-mediated silencing of *ULK3* in two different CAFs strains downmodulated key CAF effector genes and decreased *GLI1* and *GLI2* expression (Figure S5A), suggesting that *ULK3* could be an attractive target to counteract CAF activation. We tested this possibility by using the same cancer/stromal cell expansion assays discussed earlier, with parallel injections, into mouse ears, of SCC13 cells admixed with two different strains of patient-derived CAFs with or without shRNA-mediated *ULK3* silencing. As shown in Figures 6A and S5B, ear lesions formed in the presence of CAFs with *ULK3* knockdown were consistently smaller than those in corresponding CAF controls. This was paralleled by a lower number of cancer cells positive for the p63 differentiation marker and reduced ki67 proliferative index (Figure 6B). Importantly, key CAF markers such as α-Smooth Muscle Actin (SMA), Periostin (POSTN), and Tenascin C (TNC) were expressed to a much lower extent in lesions with *ULK3*-silenced CAFs than in corresponding controls, with increased macrophage infiltration and lesser angiogenesis, as assessed by antibodies against CD68 and CD31 markers, respectively (Figures 6C and S5C). These data indicate that *ULK3*, whose expression is elevated in clinically derived CAFs, is required for the tumor growth-enhancing activity of these cells.

DISCUSSION

Genes with critical cell- and tissue-regulatory functions are tightly controlled by the convergence of multiple positive and negative signals. While a large number of CAF-effector genes have been identified, an unanswered question is in regard to the integration of different signaling pathways involved in their control. In stromal fibroblasts, CSL represses senescence- and CAF-effector genes, with induction of the first class of genes occurring as the result of loss of CSL repression and increased p53 activity (Procopio et al., 2015). We show here that relief of

(H) Immunoblot analysis of HDFs infected as in (G), with antibodies against indicated proteins. n (strain) = 2.
(I) Lactate secretion in culture medium of two independent HDFs strains infected with ULK3-V5-expressing versus control viruses for 7 days. Results are expressed as ratio over control, after cell number normalization. n (strains) = 3; *p < 0.05, one sample t test.
(J) RT-PCR analysis of α-SMA (*acta2*) and tenascin (*tnc*) genes in HDF with or without siRNA-mediated silencing of *CSL* individually and in combination with *atg5*, *atg7*, or *becn1*, as indicated. n (strain) = 2. RT-PCR analysis of CAF-effector gene upregulation after *CSL* shRNA in $atg5^{+/+}$ and $atg5^{-/-}$ MEFs is in Figure S3E.
(K) qRT-PCR of the indicated genes in HDFs infected with an *atg5*-silencing virus versus control for 7 days and subsequent infection with an ULK3-V5-overexpressing and corresponding control viruses for 3 additional days (total, 10 days). Folds of expression over control; data indicate mean ± SD; n (strain) = 2.
See also Figure S3.

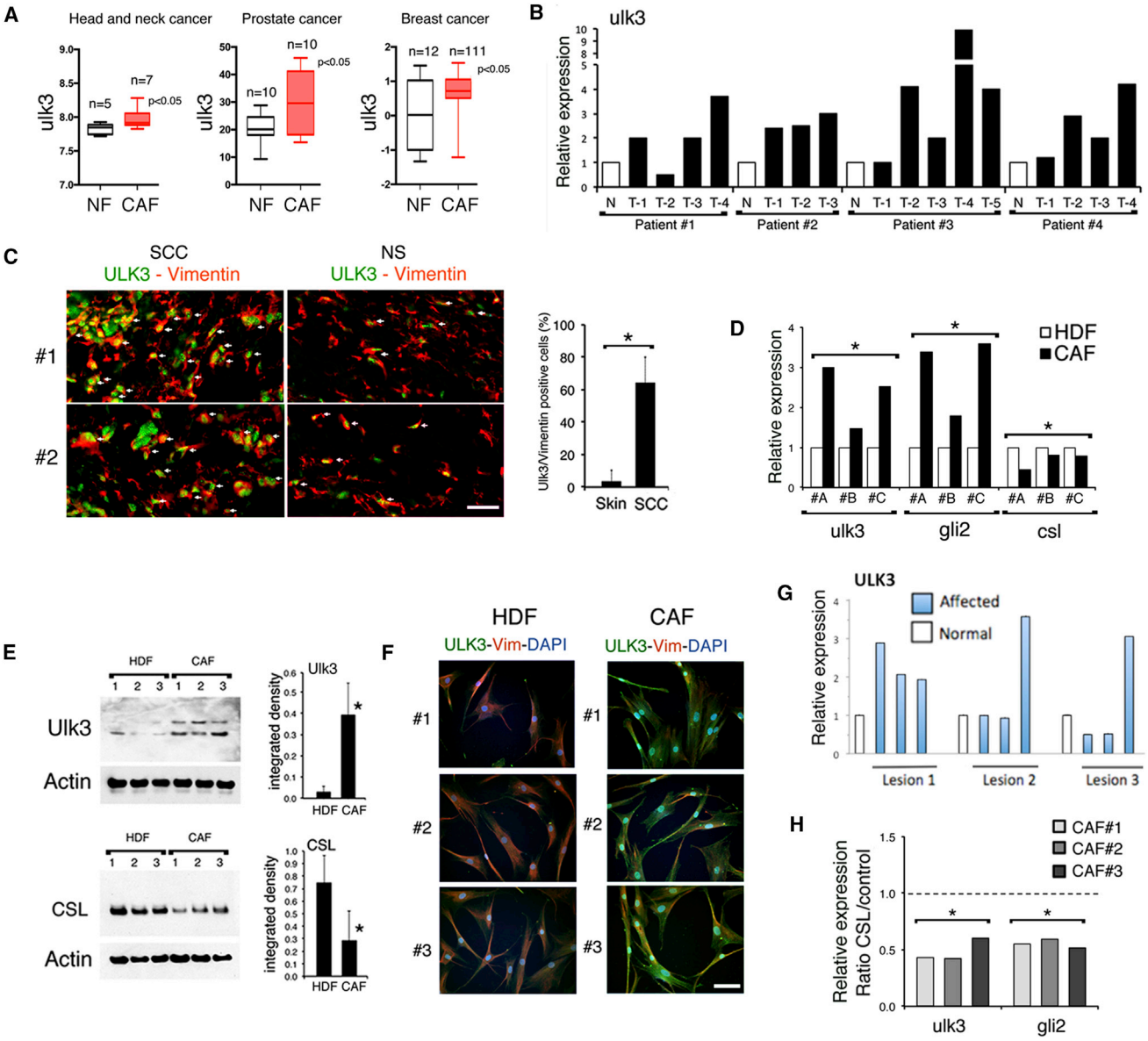

Figure 5. ULK3 Levels Are Elevated in CAFs

(A) *ULK3* levels in published gene expression profiles of CAFs derived from head/neck SCC (Costea et al., 2013), prostate cancer (Ashida et al., 2012), and breast cancer (Finak et al., 2008); head/neck, n = 7 CAFs and n = 5 healthy individuals; prostate cancer, n = 10 CAFs and n = 10 healthy patients; breast cancer, n = 111 CAFs and n = 12 healthy patients. Two class comparison t tests, *p < 0.05, NFs versus CAFs. Median, maximum (max), and (minimum (min) (vertical whiskers) are represented. The levels of *GLI1* and *GLI2* expression in these gene sets are in Figure S4A.

(B) Laser capture micro-dissection (LCM) and qRT-PCR analysis of *ULK3* expression, normalized to *36β4*, of stromal cells surrounding SCC cells versus normal skin cells from the same patient (n = 4). The captured stromal cells in the SCC areas, indicated as T-1 to T-5, were previously characterized as negative for macrophage and leukocyte infiltration and downmodulated *CSL* expression (Procopio et al., 2015).

(C) Left: double immunofluorescence analysis of stromal areas of two patient-derived squamous cell carcinomas (SCCs) and normal skin (NS) from the same individuals using anti-Vimentin (red) and anti-ULK3 (green) antibodies. Arrows point to cells double positive for vimentin and ULK3. Scale bar, 100 μm. Additional images of SCCs and NS are in Figure S4B. Right: quantification of vimentin-positive cells also ULK3^{+} in stroma of 4 NS donors compared to 4 matched and an additional 6 unmatched SCC patients. At least 100 cells were counted for each sample; ns (sample) = 10 for SCCs and 4 for NSs. *p < 0.05, two-tailed unpaired t test.

(D) qRT-PCR analysis of the indicated genes in SCC-derived CAFs versus matched normal HDFs from the same patients. n (patients) = 3. *p < 0.05, two-tailed unpaired t test.

(E) Left: immunoblotting with antibodies against ULK3, CSL, and β-actin of CAFs and HDFs from different individuals. Right: densitometric quantification; mean ± SEM. n (strains) = 3. *p < 0.05, two-tailed unpaired t test. Immunoblot of additional four CAFs and two HDFs strains is shown in Figure S4C.

(F) Immunofluorescence analysis of CAF and HDF strains as in (E), with antibodies against ULK3 (green), Vimentin (red), and DAPI (blue) staining. Scale bar, 30 μm.

(legend continued on next page)

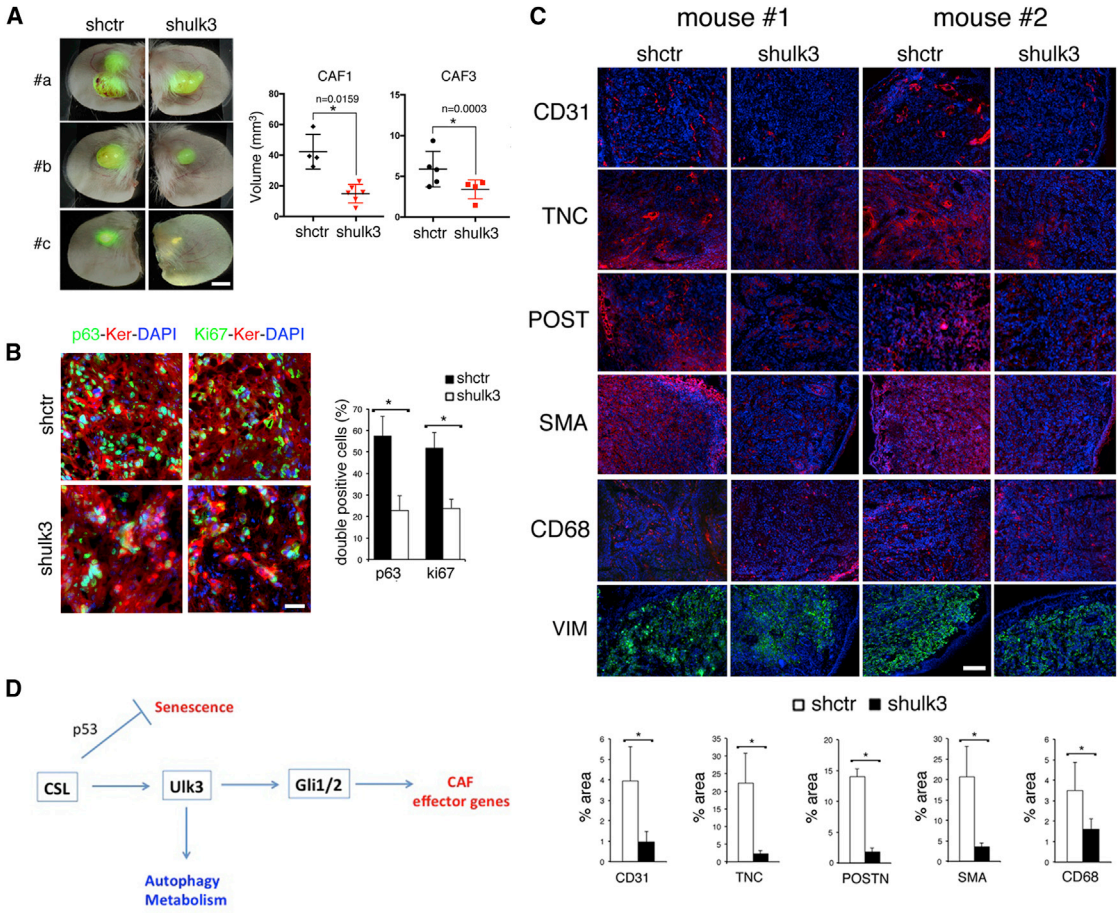

Figure 6. Loss of ULK3 Suppresses CAF Tumor-Enhancing Properties

(A) EGFP-expressing SCC13 cells admixed with two different CAFs strains (CAFs #1 and #3) infected with an *ULK3*-silencing versus control lentivirus were injected into contralateral ears of SCID mice. Left: representative bright-field and fluorescence images of three mouse ear pairs (#a, #b, and #c) 21 days after injection. Right: tumor volumes after 21 days, measured as V = (length × width^2) × 0.5, grouped by CAF strain. Data indicate median ± SD. CAF1: *shctr* versus *shulk3*, n (lesions) = 4 and 6, respectively; CAF3: *shctr* versus *shulk3*, n (lesions) = 5 and 4, respectively; unpaired samples, two-tailed equal variance t test. Scale bar, 5 mm. Matched ear pair comparisons (*shulk3*/*shctr*) are given in Figure S5B. Efficiency of *ULK3* silencing is addressed in Figure S5D.

(B) Left: immunofluorescence analysis of ear lesions formed by SCC13 cells admixed with CAFs with or without *ULK3* silencing with antibodies against p63 or ki67 (green) and pan-keratin (red) for SCC cell identification. Right: quantification of double keratin and p63- or ki67-positive cells for 3 ear pair lesions, using ImageJ and watershed segmentation of digitally acquired images. Data indicate mean ± SEM, n (animals) = 3; *p < 0.05, two-tailed unpaired t test. Scale bar, 200 μm.

(C) Top: immunofluorescence analysis of ear lesions in two animals formed by SCC13 cells admixed with *ULK3*-silenced versus control CAF1 with antibodies against endothelial (CD31) and macrophage (CD68) markers, tenascin C (TNC), α-smooth muscle actin (SMA), and periostin (POSTN), with DAPI nuclear staining. The presence of CAFs in the lesions was confirmed with anti-vimentin antibodies (VIM). Bottom: quantifications of fluorescence signal for 3 ear pair lesions, using ImageJ software; data indicate mean ± SEM; n (animals) = 3; *p < 0.05, two-tailed unpaired t test. Scale bar, 200 μM. Higher magnifications for TNC and SMA are shown in Figure S5C.

(D) Summary diagram of the process leading from normal fibroblast to CAF activation, with ULK3 as critical node, as discussed in the text.

See also Figure S5.

CSL repression of CAF-effector genes is not sufficient for induction of their expression, for which activation of GLI1/2 transcription factors is also required. Increased expression of the ULK3 kinase, which occurs in CAFs from various cancer types, provides a link between compromised CSL function and GLI activation, which can occur in concert with other previously reported Hh-receptor-dependent and -independent mechanisms (Metcalfe and de Sauvage, 2011; Seto et al., 2009; Wang et al.,

(G) RT-PCR analysis of *ULK3* expression in three LCM-obtained normal and affected stromal areas in the skin of 3 month-old mice having the CSL gene deleted. Samples were previously characterized for other genes in Procopio et al. (2015). n (lesions) = 3.

(H) qRT-PCR analysis of the indicated genes, with *36β4* for normalization, in the same CAF strains as in (E), stably infected with a doxycycline-inducible *CSL* expression or an empty-vector virus with or without doxycycline for 3 days. n (CAF) = 3; *p < 0.05, one-sample t test.

See also Figure S4.

2012; Nolan-Stevaux et al., 2009; Stecca et al., 2007). Autophagy can create a pro-tumorigenic microenvironment rich in metabolic precursors directed from CAFs to tumors (Lisanti et al., 2010; Zhao et al., 2013). As ULK3 is also an inducer of this process, it provides an attractive target for stroma-focused anti-cancer intervention to suppress combined aspects of CAF activation.

CSL is endowed with an intrinsic transcription-repressive function, and CAF-effector genes are induced as a consequence of CSL downmodulation (Hu et al., 2012; Procopio et al., 2015), as it can occur upon exposure to pro-carcinogenic stimuli such as UVA or smoke-derived compounds (Menietti et al., 2016). We show that loss of CSL transcription-repressive function is, by itself, not sufficient for induction of these genes and for the resulting tumor growth-enhancing activity of fibroblasts, for which GLI activation is needed. Aberrant activation of Hh/GLI signaling has been implicated in up to one third of all human cancers and is considered to be both a consequence and a driver of tumor-stromal interactions (Gupta et al., 2010; Ruiz i Altaba et al., 2002). Hh ligands have been implicated as paracrine mediators of cancer development (Rubin and de Sauvage, 2006). Earlier studies indicated that production of these molecules by colon, pancreatic, and ovarian cancer cells can promote tumor growth indirectly by activating Hh signaling in surrounding stroma (Theunissen and de Sauvage, 2009). However, recent evidence points to a restraining role of Hh stimulation in pancreatic and bladder cancer stroma (Özdemir et al., 2014; Rhim et al., 2014; Shin et al., 2014). In our own analysis of multiple HDFs, strains with or without *CSL* silencing, and skin-derived CAFs versus matched and unmatched controls, expression of Hh ligands was variously modulated. Similar variations were found in published profiles of CAFs from other cancer types. An attractive possibility is that, regardless of Hh levels, GLI activation in stromal fibroblasts can occur through increased activity of the ULK3 kinase, encoded by a direct CSL target gene upregulated by *CSL* downmodulation.

ULK3 was recently proposed to fulfill the same central role in mammalian cells as the *Drosophila* Fused kinase in GLI2 activation (Maloverjan et al., 2010). Besides confirming these results, we found a detectable association of endogenous ULK3-GLI2 in HDFs and showed that increased *ULK3* expression was both required and sufficient for GLI and CAF activation. Separately from this, we uncovered an interplay between CSL and ULK3 in control of autophagy that may apply, with context-dependent adjustments, to other cellular systems in which Notch signaling has been pharmacologically implicated (Barth and Köhler, 2014; Chen et al., 2016; Song et al., 2015; Yao et al., 2015). Importantly, while autophagy/mitophagy have been previously implicated in metabolic reprogramming of CAFs (Kim et al., 2011; Russell et al., 2013), our genetic evidence indicates that they are not significantly involved in the gene expression program leading to CAF activation.

A much-needed development for cancer therapy is the identification of strategies affecting cancer stroma (Goruppi and Dotto, 2013). As in HDFs with *CSL* silencing and CAFs from skin SCCs, analysis of publically available gene expression profiles indicated that *ULK3* expression is elevated in CAFs derived from several different cancer types, including HNSCC, prostate cancer, and breast cancer. Functionally, genetic suppression of *ULK3* in patient-derived CAFs was sufficient to inhibit CAF-effector gene expression as well as GLI2 activation and suppressed the growth-enhancing and pro-tumorigenic properties of these cells on neighboring cancer cells. While similar effects were observed with a compound reported to inhibit ULK3 kinase activity, further translational studies await the identification of compounds with greater specificity. Thus, ULK3 kinase, by linking two key signaling pathways involved in CAF conversion, represents an interesting target for stroma-focused anti-cancer interventions.

EXPERIMENTAL PROCEDURES

Cell Manipulations

HDFs were prepared from discarded skin samples of abdominoplasty patients at Massachusetts General Hospital (Boston, MA, USA) with institutional approval (2000P002418), or were previously obtained (Procopio et al., 2015). Conditions for culturing cells, viral infection, siRNA-mediated gene silencing, qRT-PCR, and ChIP were previously reported (Brooks et al., 2014; Hu et al., 2012). For derivation of CAFs and NFs, surgically excised discarded skin SCC samples and non-affected skin samples were dissociated with Liberase TL (Roche). For co-culture and in vivo approaches, skin SCC13 cells (Restivo et al., 2011) were infected with an EGFP-expressing lentivirus (Tiscornia et al., 2003). Each strain derived from a patient was identified with a number, which is indicated in the different panels.

Spontaneously immortalized MEFs with or without combined deletion of the *gli1* and *gli2* genes (Lipinski et al., 2008) were infected with *ULK3*-silencing or empty-vector control lentiviruses and selected with puromycin. After 2 weeks, cells were analyzed by immunofluorescence for gene expression and were then used for the in vivo studies.

Immunofluorescence, Autophagy Studies, and Cell Assays

Immunoblots and immunofluorescence analyses were performed as in (Kong et al., 2010; Procopio et al., 2015). For immunofluorescence, cells were seeded on coverslips, fixed in 3% paraformaldehyde (PFA), and processed as in Kong et al. (2010). Immunohistochemistry of tumor and tissue sections was performed as described previously (Brooks et al., 2014; Hu et al., 2012; Procopio et al., 2015), and quantification of ki67 and p63 protein levels was made using the watershed algorithm (http://imagej.nih.gov/ij/plugins/watershed.html) and ImageJ (NIH). Quantification of all other tissue immunofluorescence staining was performed using ImageJ.

Autophagosome evaluation studies were performed as in (Kong et al., 2010). Two different strains of HDFs were infected with pHcRed1-LC3 encoding for the far-red fluorescent protein (Clontech) fused to LC3.

Colorimetric determination of lactate was performed using an EnzyChrom L-Lactate Assay Kit (BioAssay Systems). The cell culture supernatants of HDFs with *CSL* silencing or overexpressing ULK3-V5 were collected after 3 days of culture. Each sample reaction was carried out in triplicate, and a standard curve of lactate was used to determine the lactate concentration.

For mitochondrial labeling, HDFs with or without *CSL* silencing for 3 days were pulse labeled with 100 nM MitoTracker Red FM (Thermo Fisher), fixed with 3% paraformaldehyde (PFA) in PBS, and analyzed using confocal microscopy (Zeiss Observer Z1) with Zen Pro 2.3 software. DAPI stained the nuclei.

The siRNA and shRNA sequences used are provided in Tables S1 and S2. The oligonucleotides used in qRT-PCR are provided in Table S3. The oligonucleotides used in ChIP experiments are provided in Table S4. A detailed list of all the antibodies and the condition(s) used is in Table S5. Unprocessed original scans of immunoblots are shown in Figures S6–S8.

Human Samples and LCM Experiments

Normal human skin samples and samples of SCC were obtained at the Department of Dermatology, Massachusetts General Hospital, as discarded parts not needed for diagnosis. All samples were processed as approved by the institutional review board. Matched normal skin and SCC paraffin samples used for

LCM and RT-PCR were provided by the Department of Dermatology, University of Tubingen, with institutional review board approvals and informed consent, as previously reported in Procopio et al. (2015). LCM was made using an Arcturus XT micro-dissection system (Applied Biosystems), as in Hu et al. (2012) and in Procopio et al. (2015). Gene expression was normalized to *36β4*, and the absence of contaminating leukocytes in the selected areas was previously confirmed with CD45 oligos in qRT-PCR assays (Procopio et al., 2015).

Animal Studies

Experiment with gli1 *and* gli2$^{-/-}$ *MEFs*

Mouse ear injections with the MEFs were carried out in 8- to 10-week-old female severe combined immunodeficiency (SCID) (CB17sc-m) mice (Taconic), as in Procopio et al. (2015). EGFP-expressing SCC13 cells (1×10^5) were admixed with equal numbers of MEFs (either *gli*$^{+/+}$ or *gli1/2*$^{-/-}$), with shRNA-mediated silencing of *CSL* or a control. Cells were injected 5 μL per site using a 33G microsyringe (Hamilton). Starting the day after injection, the mouse ears were imaged using a fluorescent stereomicroscope (Leica MZ-FLIII), every 3 days for 21 days. The mice were sacrificed after 24 days, and images of the ears were taken using bright-field and fluorescence stereomicroscopy.

Experiment with Patient-Derived CAFs

Mouse ear injections of cells were carried out in SCID mice admixing EGFP-expressing SCC13 cells (1×10^5) with equal numbers of CAFs (strain #1 or strain #3) infected with an *ULK3*-silencing lentivirus or empty-vector control. Mice were sacrificed after 3 weeks.

All animal studies were approved by the Massachusetts General Hospital Institutional Animal Care and Use Committee (2004N000170).

Statistical Analysis

Data are presented as mean ± SEM, mean ± SD, or ratios among treated and controls, with two to three separate HDFs strains in independent experiments as indicated in the figure legends. For gene expression and functional testing assays, statistical significance of differences between experimental groups and controls was assessed by two-tailed unpaired or paired t test and one sample t test. p values < 0.05 were considered as statistically significant.

SUPPLEMENTAL INFORMATION

Supplemental Information includes Supplemental Experimental Procedures, eight figures, and five tables and can be found with this article online at http://dx.doi.org/10.1016/j.celrep.2017.08.048.

AUTHOR CONTRIBUTIONS

S.G., M.-G.P., S.J., and A.C. performed the experiments and contributed to analysis of the results. V.N. provided clinical samples. S.G. and G.P.D. designed the study and wrote the manuscript.

ACKNOWLEDGMENTS

We are grateful to Robert Lipinski for the MEFs *gli1/2*$^{-/-}$ and *gli*$^{+/+}$ and to Noburo Mitzushima for the MEFs *atg5*$^{-/-}$ and *atg5*$^{+/+}$. We thank Liuqing Yang for the P-GLI2 antibodies, Alessia Di Nardo for the *shatg5* vector, Shanell Moijta for technical support with histology, and Wolfram Hoetzenecker for providing SCC samples used in LCM. A.C. is supported by a Marie Curie fellowship from the Italian Association for Cancer Research and the European Union FP7 Marie Curie Program. This work was supported by grants from the NIH (R01AR039190 and R01AR064786; the content in this paper does not necessarily represent the official views of the NIH), the Swiss National Science Foundation (310030_156191/1), and the European Research Council (26075083) to G.P.D.

Received: November 18, 2016
Revised: June 15, 2017
Accepted: August 15, 2017
Published: September 5, 2017

REFERENCES

Aberger, F., and Ruiz i Altaba, A. (2014). Context-dependent signal integration by the GLI code: the oncogenic load, pathways, modifiers and implications for cancer therapy. Semin. Cell Dev. Biol. *33*, 93–104.

Allenspach, E.J., Maillard, I., Aster, J.C., and Pear, W.S. (2002). Notch signaling in cancer. Cancer Biol. Ther. *1*, 466–476.

Artavanis-Tsakonas, S., Rand, M.D., and Lake, R.J. (1999). Notch signaling: cell fate control and signal integration in development. Science *284*, 770–776.

Ashida, S., Orloff, M.S., Bebek, G., Zhang, L., Zheng, P., Peehl, D.M., and Eng, C. (2012). Integrated analysis reveals critical genomic regions in prostate tumor microenvironment associated with clinicopathologic phenotypes. Clin. Cancer Res. *18*, 1578–1587.

Barth, J.M., and Köhler, K. (2014). How to take autophagy and endocytosis up a notch. BioMed Res. Int. *2014*, 960803.

Bingol, B., Tea, J.S., Phu, L., Reichelt, M., Bakalarski, C.E., Song, Q., Foreman, O., Kirkpatrick, D.S., and Sheng, M. (2014). The mitochondrial deubiquitinase USP30 opposes parkin-mediated mitophagy. Nature *510*, 370–375.

Bissell, M.J., and Hines, W.C. (2011). Why don't we get more cancer? A proposed role of the microenvironment in restraining cancer progression. Nat. Med. *17*, 320–329.

Brooks, Y.S., Ostano, P., Jo, S.H., Dai, J., Getsios, S., Dziunycz, P., Hofbauer, G.F., Cerveny, K., Chiorino, G., Lefort, K., and Dotto, G.P. (2014). Multifactorial ERβ and NOTCH1 control of squamous differentiation and cancer. J. Clin. Invest. *124*, 2260–2276.

Chen, X., Zhang, Y., Shi, Y., Lian, H., Tu, H., Han, S., Yin, J., Peng, B., Zhou, B., He, X., and Liu, W. (2016). MiR-129 triggers autophagic flux by regulating a novel Notch-1/ E2F7/Beclin-1 axis to impair the viability of human malignant glioma cells. Oncotarget *7*, 9222–9235.

Costea, D.E., Hills, A., Osman, A.H., Thurlow, J., Kalna, G., Huang, X., Pena Murillo, C., Parajuli, H., Suliman, S., Kulasekara, K.K., et al. (2013). Identification of two distinct carcinoma-associated fibroblast subtypes with differential tumor-promoting abilities in oral squamous cell carcinoma. Cancer Res. *73*, 3888–3901.

Dotto, G.P. (2008). Notch tumor suppressor function. Oncogene *27*, 5115–5123.

Dotto, G.P. (2009). Crosstalk of Notch with p53 and p63 in cancer growth control. Nat. Rev. Cancer *9*, 587–595.

Dotto, G.P. (2014). Multifocal epithelial tumors and field cancerization: stroma as a primary determinant. J. Clin. Invest. *124*, 1446–1453.

Finak, G., Bertos, N., Pepin, F., Sadekova, S., Souleimanova, M., Zhao, H., Chen, H., Omeroglu, G., Meterissian, S., Omeroglu, A., et al. (2008). Stromal gene expression predicts clinical outcome in breast cancer. Nat. Med. *14*, 518–527.

Goruppi, S., and Dotto, G.P. (2013). Mesenchymal stroma: primary determinant and therapeutic target for epithelial cancer. Trends Cell Biol. *23*, 593–602.

Gupta, S., Takebe, N., and Lorusso, P. (2010). Targeting the Hedgehog pathway in cancer. Ther. Adv. Med. Oncol. *2*, 237–250.

Hanahan, D., and Weinberg, R.A. (2011). Hallmarks of cancer: the next generation. Cell *144*, 646–674.

Hu, B., Castillo, E., Harewood, L., Ostano, P., Reymond, A., Dummer, R., Raffoul, W., Hoetzenecker, W., Hofbauer, G.F., and Dotto, G.P. (2012). Multifocal epithelial tumors and field cancerization from loss of mesenchymal CSL signaling. Cell *149*, 1207–1220.

Junttila, M.R., and de Sauvage, F.J. (2013). Influence of tumour micro-environment heterogeneity on therapeutic response. Nature *501*, 346–354.

Kalluri, R. (2016). The biology and function of fibroblasts in cancer. Nat. Rev. Cancer *16*, 582–598.

Kim, J., Kundu, M., Viollet, B., and Guan, K.-L. (2011). AMPK and mTOR regulate autophagy through direct phosphorylation of Ulk1. Nat. Cell Biol. *13*, 132–141.

Klionsky, D.J., Abdelmohsen, K., Abe, A., Abedin, M.J., Abeliovich, H., Acevedo Arozena, A., Adachi, H., Adams, C.M., Adams, P.D., Adeli, K., et al. (2016). Guidelines for the use and interpretation of assays for monitoring autophagy (3rd edition). Autophagy *12*, 1–222.

Kong, D.K., Georgescu, S.P., Cano, C., Aronovitz, M.J., Iovanna, J.L., Patten, R.D., Kyriakis, J.M., and Goruppi, S. (2010). Deficiency of the transcriptional regulator p8 results in increased autophagy and apoptosis, and causes impaired heart function. Mol. Biol. Cell *21*, 1335–1349.

Lipinski, R.J., Bijlsma, M.F., Gipp, J.J., Podhaizer, D.J., and Bushman, W. (2008). Establishment and characterization of immortalized Gli-null mouse embryonic fibroblast cell lines. BMC Cell Biol. *9*, 49.

Lisanti, M.P., Martinez-Outschoorn, U.E., Chiavarina, B., Pavlides, S., Whitaker-Menezes, D., Tsirigos, A., Witkiewicz, A., Lin, Z., Balliet, R., Howell, A., and Sotgia, F. (2010). Understanding the "lethal" drivers of tumor-stroma co-evolution: emerging role(s) for hypoxia, oxidative stress and autophagy/mitophagy in the tumor micro-environment. Cancer Biol. Ther. *10*, 537–542.

Maloverjan, A., Piirsoo, M., Michelson, P., Kogerman, P., and Osterlund, T. (2010). Identification of a novel serine/threonine kinase ULK3 as a positive regulator of Hedgehog pathway. Exp. Cell Res. *316*, 627–637.

Martincorena, I., Roshan, A., Gerstung, M., Ellis, P., Van Loo, P., McLaren, S., Wedge, D.C., Fullam, A., Alexandrov, L.B., Tubio, J.M., et al. (2015). Tumor evolution. High burden and pervasive positive selection of somatic mutations in normal human skin. Science *348*, 880–886.

Martinez-Outschoorn, U.E., Peiris-Pagés, M., Pestell, R.G., Sotgia, F., and Lisanti, M.P. (2017). Cancer metabolism: a therapeutic perspective. Nat. Rev. Clin. Oncol. *14*, 11–31.

Menietti, E., Xu, X., Ostano, P., Joseph, J.M., Lefort, K., and Dotto, G.P. (2016). Negative control of CSL gene transcription by stress/DNA damage response and p53. Cell Cycle *15*, 1767–1778.

Metcalfe, C., and de Sauvage, F.J. (2011). Hedgehog fights back: mechanisms of acquired resistance against Smoothened antagonists. Cancer Res. *71*, 5057–5061.

Nolan-Stevaux, O., Lau, J., Truitt, M.L., Chu, G.C., Hebrok, M., Fernández-Zapico, M.E., and Hanahan, D. (2009). GLI1 is regulated through Smoothened-independent mechanisms in neoplastic pancreatic ducts and mediates PDAC cell survival and transformation. Genes Dev. *23*, 24–36.

Özdemir, B.C., Pentcheva-Hoang, T., Carstens, J.L., Zheng, X., Wu, C.C., Simpson, T.R., Laklai, H., Sugimoto, H., Kahlert, C., Novitskiy, S.V., et al. (2014). Depletion of carcinoma-associated fibroblasts and fibrosis induces immunosuppression and accelerates pancreas cancer with reduced survival. Cancer Cell *25*, 719–734.

Procopio, M.G., Laszlo, C., Al Labban, D., Kim, D.E., Bordignon, P., Jo, S.H., Goruppi, S., Menietti, E., Ostano, P., Ala, U., et al. (2015). Combined CSL and p53 downregulation promotes cancer-associated fibroblast activation. Nat. Cell Biol. *17*, 1193–1204.

Restivo, G., Nguyen, B.C., Dziunycz, P., Ristorcelli, E., Ryan, R.J., Özuysal, O.Y., Di Piazza, M., Radtke, F., Dixon, M.J., Hofbauer, G.F., et al. (2011). IRF6 is a mediator of Notch pro-differentiation and tumour suppressive function in keratinocytes. EMBO J. *30*, 4571–4585.

Rhim, A.D., Oberstein, P.E., Thomas, D.H., Mirek, E.T., Palermo, C.F., Sastra, S.A., Dekleva, E.N., Saunders, T., Becerra, C.P., Tattersall, I.W., et al. (2014). Stromal elements act to restrain, rather than support, pancreatic ductal adenocarcinoma. Cancer Cell *25*, 735–747.

Rubin, L.L., and de Sauvage, F.J. (2006). Targeting the Hedgehog pathway in cancer. Nat. Rev. Drug Discov. *5*, 1026–1033.

Ruel, L., Rodriguez, R., Gallet, A., Lavenant-Staccini, L., and Thérond, P.P. (2003). Stability and association of Smoothened, Costal2 and Fused with Cubitus interruptus are regulated by Hedgehog. Nat. Cell Biol. *5*, 907–913.

Ruiz i Altaba, A., Sánchez, P., and Dahmane, N. (2002). Gli and hedgehog in cancer: tumours, embryos and stem cells. Nat. Rev. Cancer *2*, 361–372.

Russell, R.C., Tian, Y., Yuan, H., Park, H.W., Chang, Y.-Y., Kim, J., Kim, H., Neufeld, T.P., Dillin, A., and Guan, K.-L. (2013). ULK1 induces autophagy by phosphorylating Beclin-1 and activating VPS34 lipid kinase. Nat. Cell Biol. *15*, 741–750.

Seto, M., Ohta, M., Asaoka, Y., Ikenoue, T., Tada, M., Miyabayashi, K., Mohri, D., Tanaka, Y., Ijichi, H., Tateishi, K., et al. (2009). Regulation of the hedgehog signaling by the mitogen-activated protein kinase cascade in gastric cancer. Mol. Carcinog. *48*, 703–712.

Shin, K., Lim, A., Zhao, C., Sahoo, D., Pan, Y., Spiekerkoetter, E., Liao, J.C., and Beachy, P.A. (2014). Hedgehog signaling restrains bladder cancer progression by eliciting stromal production of urothelial differentiation factors. Cancer Cell *26*, 521–533.

Song, B.Q., Chi, Y., Li, X., Du, W.J., Han, Z.B., Tian, J.J., Li, J.J., Chen, F., Wu, H.H., Han, L.X., et al. (2015). Inhibition of Notch signaling promotes the adipogenic differentiation of mesenchymal stem cells through autophagy activation and PTEN-PI3K/AKT/mTOR pathway. Cell Physiol. Biochem. *36*, 1991–2002.

Stecca, B., Mas, C., Clement, V., Zbinden, M., Correa, R., Piguet, V., Beermann, F., and Ruiz i Altaba, A. (2007). Melanomas require HEDGEHOG-GLI signaling regulated by interactions between GLI1 and the RAS-MEK/AKT pathways. Proc. Natl. Acad. Sci. USA *104*, 5895–5900.

Theunissen, J.W., and de Sauvage, F.J. (2009). Paracrine Hedgehog signaling in cancer. Cancer Res. *69*, 6007–6010.

Tiscornia, G., Singer, O., Ikawa, M., and Verma, I.M. (2003). A general method for gene knockdown in mice by using lentiviral vectors expressing small interfering RNA. Proc. Natl. Acad. Sci. USA *100*, 1844–1848.

Wang, G., Amanai, K., Wang, B., and Jiang, J. (2000). Interactions with Costal2 and suppressor of fused regulate nuclear translocation and activity of Cubitus interruptus. Genes Dev. *14*, 2893–2905.

Wang, Y., Ding, Q., Yen, C.J., Xia, W., Izzo, J.G., Lang, J.Y., Li, C.W., Hsu, J.L., Miller, S.A., Wang, X., et al. (2012). The crosstalk of mTOR/S6K1 and Hedgehog pathways. Cancer Cell *21*, 374–387.

Xing, Z., Lin, A., Li, C., Liang, K., Wang, S., Liu, Y., Park, P., Qin, L., Wei, Y., Hawke, D., et al. (2014). lncRNA directs cooperative epigenetic regulation downstream of chemokine signals. Cell *159*, 1110–1125.

Yao, J., Zheng, K., Li, C., Liu, H., and Shan, X. (2015). Interference of Notch1 inhibits the growth of glioma cancer cells by inducing cell autophagy and down-regulation of Notch1-Hes-1 signaling pathway. Med. Oncol. *32*, 610.

Young, A.R., Narita, M., Ferreira, M., Kirschner, K., Sadaie, M., Darot, J.F., Tavaré, S., Arakawa, S., Shimizu, S., Watt, F.M., and Narita, M. (2009). Autophagy mediates the mitotic senescence transition. Genes Dev. *23*, 798–803.

Zhao, X., He, Y., and Chen, H. (2013). Autophagic tumor stroma: mechanisms and roles in tumor growth and progression. Int. J. Cancer *132*, 1–8.